Communication

High-Temperature Dehydrogenation of Brønsted Acid Sites in Zeolites

Michael J. Nash, Anne Marie Shough, Dustin W. Fickel, Douglas J. Doren, and Raul F. Lobo

J. Am. Chem. Soc., **2008**, 130 (8), 2460-2462 • DOI: 10.1021/ja709978r

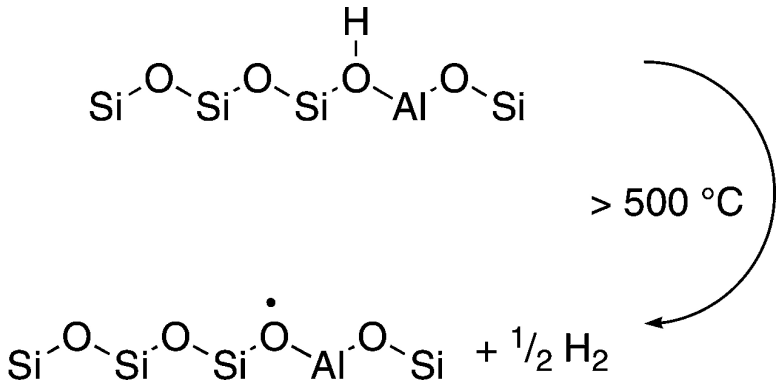

More About This Article

Additional resources and features associated with this article are available within the HTML version:

- Supporting Information
- Links to the 2 articles that cite this article, as of the time of this article download
- Access to high resolution figures
- Links to articles and content related to this article
- Copyright permission to reproduce figures and/or text from this article

View the Full Text HTML

J|A|C|S
COMMUNICATIONS

Published on Web 02/02/2008

High-Temperature Dehydrogenation of Brønsted Acid Sites in Zeolites

Michael J. Nash, Anne Marie Shough, Dustin W. Fickel, Douglas J. Doren,* and Raul F. Lobo*

Center for Catalytic Science and Technology, Department of Chemical Engineering, University of Delaware, Newark, Delaware 19716, and Department of Chemistry and Biochemistry, University of Delaware, Newark, Delaware 19716

Received November 5, 2007; E-mail: lobo@udel.edu; doren@udel.edu

Zeolites are a class of microporous aluminosilicates widely used in catalytic industrial processes as solid acids.[1] Zeolite acidity is related to the presence of the Brønsted acid sites (Si−OH−Al) in the framework.[2,3] These sites give rise to a OH vibration in the IR spectra of dehydrated samples in the 3630−3660 cm^{-1} region.[4] Early on[5] it was recognized that if a zeolite is heated above 873 K, the intensity of this vibration decreases progressively until it disappears.[6] This dehydroxylation process has been generally attributed to the dehydration of acid sites as described in Scheme 1.[5,7]

Thermally treated H-zeolites are also known to react with molecules having small ionization potentials to form stable radical cations.[7−9] There has been an intense debate regarding the composition and structure of the sites responsible for the one-electron-transfer process that forms these stable radical cations.[10] These oxidation sites are linked to the presence of Brønsted acid sites (BAS) in the zeolite[9] and not to the formation of Lewis acid sites (LAS) upon removal of aluminum from the framework and formation of extraframework aluminum species.[11] However, extraframework aluminum is usually formed during the high-temperatures needed to dehydroxilate zeolites.[12−14] The active centers are nonacidic single-electron redox sites.[15]

Here we show using mass spectrometry−temperature-programmed desorption (MS−TPD) that the product of heating high-silica H-zeolites is predominantly hydrogen. Using electronic-structure calculations we also show a plausible path for the formation of hydrogen from zeolite BAS (Scheme 2) and propose that the reaction should lead to the formation of $[AlO_4]^0$ sites in the zeolite.[16] These $[AlO_4]^0$ sites can act as nonacidic one-electron acceptors of adsorbed molecules (as suggested by Shih[8]) and could react further to form a more stable species. As such these sites could play an important role in the catalytic chemistry of hydrocarbons at high temperatures (see below).

Figure 1 shows the MS−TPD traces of $m/e = 2$ (H_2) and $m/e = 18$ (water) desorbed from two samples of H-ZSM-5 ($SiO_2/Al_2O_3 = 20$, 40) under helium flow (see Supporting Information for experimental details). During the initial heating to 250 °C (not shown) only water is desorbed. However, during the last temperature ramp to 750 °C a substantial amount of hydrogen is observed simultaneously with a small amount of water. Clearly, the sample of ZSM-5 with $SiO_2/Al_2O_3 = 20$ produces more hydrogen than a similar amount of ZSM-5 with $SiO_2/Al_2O_3 = 40$. Zeolites H-β and H-mordenite ($SiO_2/Al_2O_3 = 18$) also produce hydrogen upon heating. The process is irreversible since a sample of H-mordenite ($SiO_2/Al_2O_3 = 18$) heated to 750 °C, cooled to 500 °C, and reheated to 750 °C produces hydrogen in the first temperature ramp only. Samples with higher aluminum content (H−Y, $SiO_2/Al_2O_3 = 5$, H-mordenite $SiO_2/Al_2O_3 = 10.4$) produce hydrogen but also produce much more water. We conducted a series of control experiments to ensure that this signal is not an experimental artifact (see Supporting Information). The empty reactor and the reactor containing the sample support (fused quartz chips) produce no hydrogen signal. Samples of Na-mordenite also produce no hydrogen upon heating.

Scheme 1. Dehydroxilation of Brønsted Acid Sites by Dehydration

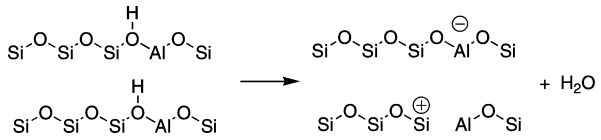

Scheme 2. Homolytic Decomposition of Brønsted Acid Sites

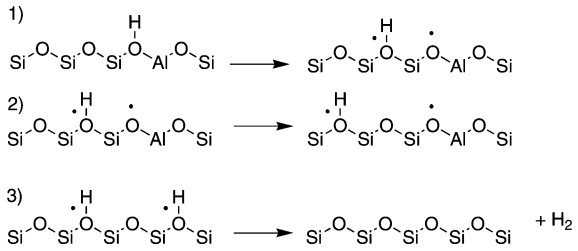

The two samples of ZSM-5 used in the MS−TPD experiments were prepared using a synthesis gel containing no organic structure directors.[17] This is an important consideration because ZSM-5 samples prepared using tetrapropylammonium usually have missing T-atoms (Si or Al) in the framework that lead to the formation of hydroxyl nests.[18,19] These sites also react at high temperatures producing hydrogen and bis-silylperoxo groups in the zeolite framework.[20,21] In fact, silicalite-1 produces more hydrogen gas than ZSM-5 ($SiO_2/Al_2O_3 = 20$) because each hydroxyl nest produces two hydrogen molecules and there is approximately one defect per channel intersection.

The weak water signal during the last ramp in the TPD of Figure 1 indicates that the reaction of Scheme 1[22] is not prevalent and that different chemistry occurs during heating. A homolytic bond-breaking process (Scheme 2) could explain the results of Figure 1. The first step is the dissociation of the OH bond of the BAS to form hydrogen atoms adsorbed on adjacent framework oxygen atoms and a $[AlO_4]^0$ site (step 1). This is followed by diffusion of the hydrogen atoms (step 2) and finally the recombination of two H atoms to form molecular hydrogen. H atoms trapped in zeolite cavities and $[AlO_4]^0$ defects have both been observed by ESR in γ-irradiated H-zeolites,[23] and there is extensive experimental[24] and theoretical[25] evidence for the presence of $[AlO_4]^0$ defects in quartz. Note that in all cases we find small amounts of water desorbed at high temperatures and that the reaction depicted in Scheme 1 (or some similar process) can occur simultaneously with the dehydrogenation. This explains the formation of LAS in dehydroxylated ZSM-5 samples treated under similar conditions to the ones used here.[6,12]

The formation and properties of $[AlO_4]^0$ sites in quartz have been investigated extensively.[26−29] Formally they can more clearly be

10.1021/ja709978r CCC: $40.75

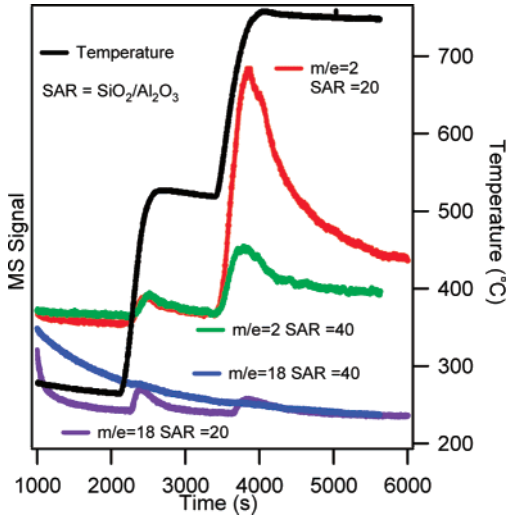

Figure 1. MS−TPD traces of water ($m/e = 18$) and hydrogen ($m/e = 2$) for two samples of zeolite H-ZSM-5 in flowing helium (1 bar). The temperature profile corresponds to ZSM-5 with $SiO_2/Al_2O_3 = 20$, the other being nearly the same.

Table 1. Reaction Energies Predicted for Scheme 2

step	description	ΔE (kcal/mol)
1	O−H bond dissociation and H diffusion	28.7
2	H diffusion (first to second coordination sphere)	4.5
3	$^1/_2H_2$ association (from second coordination sphere)	30.4

described as $[AlO_4/h]^0$ where h is a hole located (at low temperatures) on one of the oxygen atoms surrounding the aluminum, that is, one oxygen atom is oxidized to a formal oxidation state of 1−. These $[AlO_4]^0$ sites can be formed starting with $[AlO_4]^-M^+$ (M = Na^+) which substitutes for Si in quartz, sweeping with hydrogen in an electric field to form $[AlO_4]^-H^+$ (i.e., BAS) and heating in vacuum (1400 K) whereby internal OH groups dissociate producing hydrogen.[30,31] Quartz samples treated in this form are ESR silent and the $[AlO_4]^0$ sites are only observed after irradiation with X-rays or γ-rays.[32] The ESR spectroscopy of the $[AlO_4]^0$ site at 77 K shows that the unpaired electron (likewise, the hole) is localized on an oxygen atom.[24] At room temperature the hole h associated with this paramagnetic electron jumps rapidly between the four chemically equivalent oxygen atoms of the $[AlO_4]^0$ site broadening the ESR signal.[33] Furthermore, irradiated quartz samples thermoluminesce (at ∼110 °C) suggesting $[AlO_4]^0$ sites are not the most stable electronic structure of the system.[32] The structure of the oxidized sites in the more stable state after thermoluminescence is unknown.[31]

The H-zeolite samples investigated here behave similarly to quartz samples with aluminum impurities. Besides producing hydrogen, we have also found that upon dehydrogenation our samples (H-mordenite and H-ZSM-5) are ESR silent (see also refs 11,15). This is consistent with reports where X-ray or γ-ray irradiation is required to produce the ESR signals assigned to $[AlO_4]^0$ sites in quartz. This provides further evidence that the ground state is not composed of $[AlO_4]^0$ sites. Presumably, the structure of this unknown ground state is similar to the one formed in quartz.

We have investigated the energetics and structures for the reactions in Scheme 2 using ZSM-5 cluster models with 188 T-atoms, optimized with hybrid quantum mechanics/molecular mechanics (QM/MM) methods. Details on the computational methods can be found in Supporting Information. From the reaction energies, (ΔE, Table 1), the predicted overall ΔE for Scheme 2

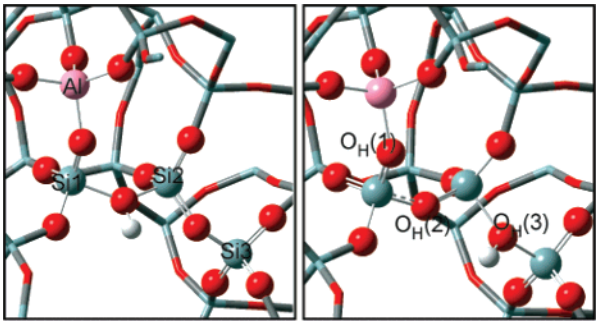

Figure 2. Optimized local structures surrounding O_H sites for the products of step 1 and 2 in Scheme 2. Portions of this model have been shown in stick form to facilitate the visualization of the O_H sites.

Table 2. Values of $\Delta\Phi_k$ for Each O Acid Binding Site in Steps 1 and 2 for Scheme 2

	$\Delta\Phi_k$	
	step 1 $O_H(1) \rightarrow O_H(2)$	step 2 $O_H(2) \rightarrow O_H(3)$
$O_H(1)$	−0.2468	0.0437
$O_H(2)$	0.2792	−0.1867
$O_H(3)$	0.0490	0.1850

per OH site is 65.8 kcal/mol where step 3 is tentatively identified as the rate-determining step.

The geometries surrounding each O−H binding site, O_H, in steps 1 and 2, are similar to those reported by Franke et al.[34] As the H diffuses away from the BAS site the $O_H(1)$−Al bond is shortened from 1.89 to 1.75 Å, along with an increase in all $\angle O_H(1)$−Al−O, resulting in a tetrahedrally coordinated AlO_4 site (see Figure 2). On the other hand, as H diffuses into a Si−O_H−Si environment the opposite is observed. The Si−O_H bond lengths to which the H atom is bound increase, along with a decrease in the $\angle O_H$−Si−O. Upon H_2 association (step 3), the hole state becomes localized on a single O atom bonded to the Al site with a geometric and electronic structure similar to that predicted by others.[25,29] A complete description of the local geometry for each step in Scheme 2 can be found in Supporting Information.

The diffusion process in Scheme 2 is proposed to be that of a H atom, not a proton as previously suggested by Franke et al.[34] This distinction can be made on the basis of changes in orbital occupations between each diffusion step. We define $\Delta\Phi_k$ as the summed difference of gross orbital populations for a given atom k

$$\Delta\Phi_k = \sum_i^n \phi_{i,k}^{\text{final}} - \sum_i^n \phi_{i,k}^{\text{initial}} \qquad (1)$$

where $\phi_{i,k}^{\text{initial}}$ and $\phi_{i,k}^{\text{final}}$ are the populations of atomic orbital i for atom k in the initial and final structures for a given diffusion step, respectively. The $\Delta\Phi_k$ values for each O atom binding site, O_H, in steps 1 and 2 of Scheme 2 are reported in Table 2. If a *proton* were diffusing from O_H(initial) to O_H(final), breaking the O_H-(initial)−H bond would shift orbital occupation from the H^+ to the O_H(initial) thus increasing the gross orbital population of O_H-(initial). Similarly, as the proton forms a new bond with O_H(final) orbital occupation will shift from O_H(final) to the proton decreasing the gross orbital population of O_H(final). However, this is the opposite of what is observed in the optimized models (Table 2). In step 1 as the H moves from $O_H(1)$ to $O_H(2)$, a decrease in $\Delta\Phi_{O_H(1)}$ correlates with an increase in $\Delta\Phi_{O_H(2)}$ of a similar magnitude. For this step the value of $\Delta\Phi_{O_H(3)}$ is effectively zero as it does not contribute to H bonding. The same trend occurs for step 2 with

orbital occupation being shifted from $O_H(2)$ to $O_H(3)$, while occupation on $O_H(1)$ remains nearly unchanged. These changes in gross orbital populations are consistent with diffusion of a H atom, removing orbital occupation from O_H(initial) and repositioning it on O_H(final) to form a new O−H bond.

The ΔE reported for steps 1 and 2 in Table 1 are similar to those reported by Franke et al.[34] for proton diffusion between two Al sites in ZSM-5. The small differences (4−7 kcal/mol) may be due to the different methodologies and ZSM-5 models employed. This suggests that both theoretical studies probe the same diffusion process. The above analysis of $\Delta\Phi_k$ presents evidence for simultaneous diffusion of an electron with the hydrogen species, supporting the assignment of the diffusing entity to a H atom.

A recent Al-EXAFS investigation[35] of the thermal treatment of H-mordenite shows that after dehydrogenation the aluminum remains in the zeolite framework. Bugaev et al.[35] observed that the framework aluminum atoms are in the expected distorted tetrahedral geometry of a BAS upon dehydration at 573 K (in vacuum) but that upon heating to 985 K (i.e., dehydroxylation) the alumina tetrahedra become very uniform. This geometry is consistent with a $[AlO_4]^0$ site where the unpaired electron is delocalized among the four oxygen atoms surrounding the aluminum, also consistent with the broadening of the ESR signal.[33] Unpaired electrons in $[AlO_4]^0$ sites will greatly broaden the ^{27}Al NMR signal of framework aluminum through paramagnetic interactions and may also explain the lack of detection of the so-called NMR invisible aluminum species[36] reported in dehydroxylated zeolites.[13]

The sites formed upon dehydrogenation are oxidation sites and are likely the destination of the electrons abstracted from organic molecules that form radical cations in zeolite pores. It has been puzzling that upon formation of the radical cations in zeolites, there has been no direct evidence by ESR of the abstracted electrons.[10] This issue is resolved by recognizing that upon electron abstraction an $[AlO_4]^0$ site is reduced to $[AlO_4]^-$, the normal oxidation state of the zeolite framework that should not, of course, give rise to an ESR signal. It has also been reported that molecular oxygen can accelerate the rate of formation of one-electron oxidation sites.[10,15] This is not surprising since formally the dehydrogenation of BAS (Scheme 2) results in the oxidation of the framework. The reaction of O_2 with BAS to form water[8] and $[AlO_4]^0$ sites should occur at lower temperatures than the dehydrogenation observed here.

Given the rapid rate of dehydrogenation of BAS above 873 K (Figure 1) it is tempting to speculate on the role of the resulting redox sites in fluidized catalytic cracking (FCC). Prior to contacting the hydrocarbons in the FCC riser, the catalyst particles spend tens of minutes at 945−1000 K under oxidizing conditions in the FCC regenerator. On the basis of the results reported here, it would be expected that a large fraction of the BAS of the catalysts particles would be dehydrogenated at the point of contact of catalysts and hydrocarbons. The catalytic chemistry observed in the early portions of the FCC riser could be greatly affected by radical cation intermediates formed by interaction with redox sites[37,38] in addition to surface alkoxide intermediates.[39] It is possible that BAS dehydrogenation is the first step toward the formation of extraframework aluminum by steaming at high temperatures.

Acknowledgment. This research was supported by the US Department of Energy under Grant No. DE-FG02-99ER14998. We thank K. Al-Majnouni for preparing the mordenite samples.

Supporting Information Available: Sample synthesis and characterization, description of the TPD protocols and control experiments, and details of the electronic structure calculations. This material is available free of charge via the Internet at http://pubs.acs.org.

References

(1) Tanabe, K.; Holderich, W. F. *Appl. Catal., A* **1999**, *181*, 399−434.
(2) Corma, A. *Chem. Rev.* **1995**, *95*, 559−614.
(3) vanSanten, R. A. *Catal. Today* **1997**, *38*, 377−390.
(4) Paze, C.; Bordiga, S.; Lamberti, C.; Salvalaggio, M.; Zecchina, A.; Bellussi, G. *J. Phys. Chem. B* **1997**, *101*, 4740−4751.
(5) Uytterhoeven, J. B.; Christner, L. G.; Hall, W. K. *J. Phys. Chem.* **1965**, *69*, 2117.
(6) Szanyi, J.; Paffett, M. T. *Microporous Mater.* **1996**, *7*, 201−218.
(7) Stamires, D. N.; Turkevich, J. *J. Am. Chem. Soc.* **1964**, *86*, 749-757.
(8) Shih, S. *J. Catal.* **1983**, *79*, 390−395.
(9) Cano, M. L.; Corma, A.; Fornes, V.; Garcia, H. *J. Phys. Chem.* **1995**, *99*, 4241−4246.
(10) Garcia, H.; Roth, H. D. *Chem. Rev.* **2002**, *102*, 3947−4007.
(11) Harvey, G.; Prins, R.; Crockett, R.; Roduner, E. *J. Chem. Soc., Faraday Trans.* **1996**, *92*, 2027−2033.
(12) Kustov, L. M.; Kazansky, V. B.; Beran, S.; Kubelkova, L.; Jiru, P. *J. Phys. Chem.* **1987**, *91*, 5247−5251.
(13) van Bokhoven, J. A.; van der Eerden, A. M. J.; Koningsberger, D. C. *J. Am. Chem. Soc.* **2003**, *125*, 7435−7442.
(14) Kanellopoulos, J.; Unger, A.; Schwieger, W.; Freude, D. *J. Catal.* **2006**, *237*, 416−425.
(15) Leu, T. M.; Roduner, E. *J. Catal.* **2004**, *228*, 397−404.
(16) Solans-Monfort, X.; Branchadell, V.; Sodupe, M.; Sierka, M.; Sauer, J. *J. Chem. Phys.* **2004**, *121*, 6034−6041.
(17) Kim, S. D.; Noh, S. H.; Seong, K. H.; Kim, W. J. *Micropor. Mesopor. Mater.* **2004**, *72*, 185.
(18) Zecchina, A.; Bordiga, S.; Spoto, G.; Marchese, L.; Petrini, G.; Leofanti, G.; Padovan, M. *J. Phys. Chem.* **1992**, *96*, 4991−4997.
(19) Bordiga, S.; Ugliengo, P.; Damin, A.; Lamberti, C.; Spoto, G.; Zecchina, A.; Spano, G.; Buzzoni, R.; Dalloro, L.; Rivetti, F. *Topcis Catal.* **2001**, *15*, 43−52.
(20) Fickel, D. W.; Shough, A. M.; Nash, M. J.; Doren, D. J.; Lobo, R. F. *Chem. Mater.* **2007**, submitted for publication.
(21) Sokol, A. A.; Catlow, C. R. A.; Garces, J. M.; Kuperman, A. *J. Phys.: Condens. Matter.* **2004**, *16*, S2781−S2794.
(22) Catlow, C. R. A.; Sinclair, P. E.; Sokol, A. A. *Radiat. Eff. Defect Solids* **1999**, *151*, 235−241.
(23) Aboukais, A.; Vedrine, J. C.; Massardier, J. **1975**, *71*, 1697−1706.
(24) Nuttall, R. H. D.; Weil, J. A. *Can. J. Phys.* **1981**, *59*, 1696−1708.
(25) To, J.; Sokol, A. A.; French, S. A.; Kaltsoyannis, N.; Catlow, C. R. A. *J. Chem. Phys.* **2005**, *122*.
(26) Koumvakalis, N. *J. Appl. Phys.* **1980**, *51*, 5528−5532.
(27) Itoh, N.; Stoneham, D.; Stoneham, A. M. *J. Appl. Phys.* **2002**, *92*, 5036−5044.
(28) Martini, M.; Meinardi, F.; Vedda, A. *Radiat. Meas.* **2000**, *32*, 673−677.
(29) Pacchioni, G.; Frigoli, F.; Ricci, D.; Weil, J. A. *Phys. Rev. B* **2001**, *6305*.
(30) Campone, P.; Spinolo, G.; Vedda, A.; Checchetto, R.; Gratton, L. M.; Miotello, A.; Tomasi, A. *Solid State Commun.* **1996**, *98*, 917−922.
(31) Checchetto, R.; Miotello, A.; Tomasi, A. *Chem. Phys. Lett.* **1999**, *306*, 330−334.
(32) Martini, M.; Paleari, A.; Spinolo, G.; Vedda, A. *Phys. Rev. B* **1995**, *52*, 138−142.
(33) Schnadt, R.; Rauber, A. *Solid State Commun.* **1971**, *9*, 159.
(34) Franke, M. E.; Sierka, M.; Simon, U.; Sauer, J. *Phys. Chem. Chem. Phys.* **2002**, *4*, 5207−5216.
(35) Bugaev, L. A.; van Bokhoven, J. A.; Sokolenko, A. P.; Latokha, Y. V.; Avakyan, L. A. *J. Phys. Chem. B* **2005**, *109*, 10771−10778.
(36) Freude, D.; Ernst, H.; Wolf, I. *Solid State Nucl. Magn. Reson.* **1994**, *3*, 271−286.
(37) Corma, A.; Fornes, V.; Martinez, A.; Orchilles, A. V. *ACS. Symp. Ser.* **1988**, *368*, 542−554.
(38) McVicker, G. B.; Kramer, G. M.; Ziemiak, J. J. *J. Catal.* **1983**, *83*, 286−300.
(39) Corma, A.; Orchilles, A. V. *Microporous Mesoporous Mater.* **2000**, *35−6*, 21−30.

JA709978R